Dynamic Model for 3-D Magnetostrictive Transducers

Phillip G. Evans[1] and Marcelo J. Dapino[2]

[1]Lincoln Laboratory, Massachusetts Institute of Technology, Lexington, MA 02420-9108 USA
[2]Department of Mechanical & Aerospace Engineering, The Ohio State University, Columbus, OH 43210 USA

A comprehensive analytical framework is developed for the study of magnetostrictive transducers with arbitrary geometries operated in dynamic regimes. Weak form equations are derived from Maxwell's equations and linear momentum without restricting the form of the constitutive behavior of the magnetostrictive material. For validation, the framework is implemented for a unimorph beam actuator which has both active and passive media.

Index Terms—**Finite-element modeling, Galfenol, magnetostrictive transducers, nonlinear modeling.**

I. Introduction

GALFENOL (Fe-Ga) is an emerging magnetostrictive material which can exhibit moderate magnetostriction and mechanical properties similar to steel. These unique characteristics offer the possibility of creating structural elements or fasteners with actuation and sensing properties. Actuators have been proposed that exploit the mechanical robustness of Galfenol [1], [2], but the development of structures with integrated 3-D actuation and sensing has not been fully explored. While 3-D models for Galfenol constitutive behavior have been developed [3]–[5], a general model for 3-D dynamic behavior of Galfenol-driven systems is still necessary.

Transducer-level models are useful for device design, optimization, and control [6]–[9]. Much attention has been given to devices utilizing Terfenol-D loaded unidirectionally. Dapino *et al.* [10] employed the Jiles-Atherton model augmented by an effective field due to prestress to model the 1-D constitutive behavior of Terfenol-D. The magnetostriction calculated from the constitutive model is used as input to the wave equation for the structural dynamics of a rod. Huang *et al.* [11] also used the Jiles-Atherton model for 1-D characterization of a Terfenol-D actuator but included eddy-current losses in the energy formulation and used a lumped parameter model for the structural dynamics; the effect of dynamic stress was not considered. Sarawate and Dapino [12] developed a decoupled model which included time delay from eddy currents through solution of the magnetic field diffusion equation with constant permeability. Engdahl and Bergqvist [13] calculated dynamic losses in a 1-D actuator by fully coupling the magnetic field diffusion equation, the wave equation for structural dynamics, and a lumped parameter model for the magnetic circuit. Bottauscio *et al.* [14] modeled losses from eddy currents using the field diffusion equation along with the Preisach model to calculate the nonlinear permeability and stress-induced flux density changes. All of these models employ the externally applied magnetic field as an input.

Manuscript received February 15, 2010; revised June 15, 2010 and August 09, 2010; accepted October 09, 2010. Date of publication October 18, 2010; date of current version December 27, 2010. Corresponding author: M. J. Dapino (e-mail: dapino.1@osu.edu).

Color versions of one or more of the figures in this paper are available online at http://ieeexplore.ieee.org.

Digital Object Identifier 10.1109/TMAG.2010.2088130

Some attention has also been given to higher-dimension models. Datta *et al.* [15], [16] used classical laminated plate theory with the Armstrong magnetomechanical model to characterize laminated sensors and actuators in the absence of current-induced magnetic fields. Zhou and Zhou [17] developed a dynamic finite-element model for a unimorph actuator with one-way magnetomechanical coupling. The 2-D magnetostatic finite-element model formulated by Kannan and Dasgupta [18] utilizes a nonlinear constitutive behavior for bidirectional coupling and includes current-induced magnetic fields and electromagnetic body forces. Mudivarthi *et al.* [19] formulated a fully-coupled, magnetostatic formulation for stress-induced flux density changes in Galfenol with no current-induced fields. The 3-D model of Kim and Jung [20] employs one-way coupling with force due to magnetostriction driving a coupled fluid-structural model for a sonar transducer. Aparicio and Sosa presented a 3-D [21], fully-coupled finite-element model including dynamic effects and implemented it for a magnetostrictive material using a single element.

This work provides a comprehensive analytical framework for design and characterization of 3-D magnetostrictive transducers. The effects of eddy currents, structural dynamics, flux leakage, and nonlinear magnetostrictive behavior are simultaneously included. A general implementation is given which includes surrounding air and current-carrying coils, and describes the full input-output relationship in 3-D between voltage, force, and displacement. The framework is demonstrated by analyzing the step response of a 3-D unimorph actuator with a linear material model.

II. Model Development

A. Governing Equations

The behavior of an electro-magneto-mechanical system is governed by Maxwell's equations and the conservation of linear momentum. The point-wise or strong form equation for the spatial and temporal dependence of magnetic field $\mathbf{H}$ is

$$\nabla \times \mathbf{H} = \mathbf{J}_s + \mathbf{J}_E \tag{1}$$

$$\mathbf{J}_E = -\sigma \frac{\partial \mathbf{A}}{\partial t} \tag{2}$$

when displacement current is negligible, as is typical for the operating range of magnetostrictive transducers

(<30 MHz). Equation (1) represents both Ampère's law and the Lenz-Faraday law for ohmic materials with conductivity σ. The total current density is the source $\mathbf{J}_s$ from an applied voltage and the eddy-current term $\mathbf{J}_E$. The eddy-current term is expressed with the ungauged vector magnetic potential $\mathbf{A}$, defined from the magnetic flux density $\mathbf{B}$

$$\mathbf{B} = \nabla \times \mathbf{A}. \tag{3}$$

The strong form governing the spatial and temporal dependence of displacement $\mathbf{u}$ and stress $\mathbf{T}$ is

$$\rho \frac{\partial^2 \mathbf{u}}{\partial t^2} + c\frac{\partial \mathbf{u}}{\partial t} = \nabla \cdot \mathbf{T} + \mathbf{f}_B \tag{4}$$

where ρ is density, c is viscous damping per volume, and $\mathbf{f}_B$ is body force per volume. The infinitesimal strain is kinematically related to displacement according to

$$\mathbf{S} = \nabla \mathbf{u}. \tag{5}$$

The weak form equations, approximately solved by the finite-element method in Section II-B, are obtained by weighting (1) and (4) with $\delta\mathbf{A}$ and $\delta\mathbf{u}$ (see Appendix A)

$$\int_{V_B} \mathbf{H} \cdot (\nabla \times \delta\mathbf{A})\, dV + \int_{V_B} \sigma \frac{\partial \mathbf{A}}{\partial t} \cdot \delta\mathbf{A}\, dV = \int_{\partial V_B} (\mathbf{H} \times \mathbf{n}) \cdot \delta\mathbf{A}\, d\partial V + \int_{V_B} \mathbf{J}_s \cdot \delta\mathbf{A}\, dV \tag{6}$$

$$\int_{V_u} \mathbf{T} \cdot \nabla\delta\mathbf{u}\, dV + \int_{V_u} \rho \frac{\partial^2 \mathbf{u}}{\partial t^2} \cdot \delta\mathbf{u}\, dV + \int_{V_u} c\frac{\partial \mathbf{u}}{\partial t} \cdot \delta\mathbf{u}\, dV = \int_{\partial V_u} \mathbf{T}\mathbf{n} \cdot \delta\mathbf{u}\, d\partial V + \int_{V_u} \mathbf{f}_B \cdot \delta\mathbf{u}\, dV. \tag{7}$$

The weak form represents a balance of the internal and external virtual work, since the kinematic relationships $\delta\mathbf{B} = \nabla \times \delta\mathbf{A}$ and $\delta\mathbf{S} = \nabla\delta\mathbf{u}$ appear as work conjugates with $\mathbf{H}$ and $\mathbf{T}$. Additionally, the surface traction at the mechanical boundary is $\mathbf{t} = \mathbf{T}\mathbf{n}$ and the tangent field at the magnetic boundary is $\mathbf{H}_T = \mathbf{H} \times \mathbf{n}$. With these relationships, the system equations become

$$\int_{V_B} \mathbf{H} \cdot \delta\mathbf{B}\, dV + \int_{V_B} \sigma \frac{\partial \mathbf{A}}{\partial t} \cdot \delta\mathbf{A}\, dV = \int_{\partial V_B} \mathbf{H}_T \cdot \delta\mathbf{A}\, d\partial V + \int_{V_B} \mathbf{J}_s \cdot \delta\mathbf{A}\, dV \tag{8}$$

$$\int_{V_u} \mathbf{T} \cdot \delta\mathbf{S}\, dV + \int_{V_u} \rho \frac{\partial^2 \mathbf{u}}{\partial t^2} \cdot \delta\mathbf{u}\, dV + \int_{V_u} c\frac{\partial \mathbf{u}}{\partial t} \cdot \delta\mathbf{u}\, dV = \int_{\partial V_u} \mathbf{t} \cdot \delta\mathbf{u}\, d\partial V + \int_{V_u} \mathbf{f}_B \cdot \delta\mathbf{u}\, dV. \tag{9}$$

These virtual work expressions describe both coupled and uncoupled systems. Coupling occurs in systems with active materials, having coupled constitutive behavior for magnetic field, flux density, stress, and strain. Though magnetomechanical coupling can occur in systems having only passive materials, through the Lorentz force as in moving-iron systems, the effect is negligible for the small motions typical of magnetostrictive actuators and sensors and is not considered here.

B. 3-D Finite-Element Formulation

In the finite-element method, the solution domain is discretized into finite elements and the integrations in the weak form (6) and (7) are performed over elements. The solution variables, vector potential, and displacement in the element are interpolated from the nodal values. Therefore, only the interpolation or shape functions are integrated resulting in matrix equations for the nodal values of the vector potential and displacement, stored in the vectors $\mathbf{Q}^A$ and $\mathbf{Q}^u$, respectively. For passive electromagnetic systems, it is increasingly common to use edge elements for the magnetic field rather than a nodal formulation with the ungauged vector magnetic potential. While this leads to better conditioned matrices, the nodal formulation is used here to enable coupling with mechanical variables.

The structure of the finite-element model contributes to the understanding of coupled magnetomechanical systems operated under electromagnetically quasi-static conditions

$$\begin{bmatrix} \mathbf{0} & \mathbf{0} \\ \mathbf{0} & \mathbf{M}^u \end{bmatrix} \begin{pmatrix} \ddot{\mathbf{Q}}^A \\ \ddot{\mathbf{Q}}^u \end{pmatrix} + \begin{bmatrix} \mathbf{D}^A & \mathbf{0} \\ \mathbf{0} & \mathbf{D}^u \end{bmatrix} \begin{pmatrix} \dot{\mathbf{Q}}^A \\ \dot{\mathbf{Q}}^u \end{pmatrix} + \begin{bmatrix} \mathbf{K}^A & -\mathbf{K}^{uA} \\ -(\mathbf{K}^{uA})^T & \mathbf{K}^u \end{bmatrix} \begin{pmatrix} \mathbf{Q}^A \\ \mathbf{Q}^u \end{pmatrix} = \begin{pmatrix} \mathbf{F}^A \\ \mathbf{F}^u \end{pmatrix}. \tag{10}$$

The mass matrix is singular, containing only contributions from the mechanical mass, $\mathbf{M}^u$. The absence of entries from the electromagnetic domain is a consequence of neglecting Maxwell's displacement current and prevents the finite-element model from characterizing electromagnetic radiation, which does not occur in the typical operating regime of magnetostrictive devices (<30 MHz). Sources of damping include the internal material damping (mechanical) which yields $\mathbf{D}^u$ and eddy currents which give rise to $\mathbf{D}^A$. The magnetic stiffness $\mathbf{K}^A$ depends on magnetic permeability and characterizes the ability of the system to magnetically energize the system. The coupling matrix $\mathbf{K}^{uA}$ characterizes the ability of the system to transfer mechanical energy, applied through surface tractions in the mechanical load vector $\mathbf{F}^u$, to magnetic energy and conversely, to transform magnetic energy, applied through current in the magnetic load vector $\mathbf{F}^A$, to mechanical energy. The derivation of these matrices is shown in Appendix B.

C. 3-D Dynamic Implementation

In this section, a unimorph actuator (Fig. 1) is studied with the fully 3-D and dynamic finite-element model (10). The model is implemented in COMSOL Multiphysics which provides a meshing tool, local to global matrix assembly, and a post-processing and visualization toolbox. This software allows for partitioning the solution domain while allowing for the different subdomains to have different degrees of freedom. COMSOL

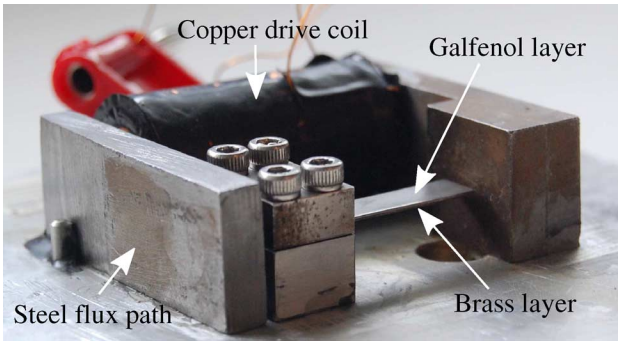

Fig. 1. Unimorph actuator employed for model validations.

Multiphysics also allows specifying essential boundary conditions on internal boundaries, which is important because the mechanical constraints are inside the surrounding air volume.

The coefficient matrices in (51) and (52) for magnetostrictive material behavior can in general be calculated from a nonlinear constitutive model, for example the efficient model [5]. Constitutive models are most commonly formulated as

$$\mathbf{B} = \mathbf{B}(\mathbf{H}, \mathbf{T}) \tag{11}$$

$$\mathbf{S} = \mathbf{S}(\mathbf{H}, \mathbf{T}) \tag{12}$$

with derivatives

$$\boldsymbol{\mu} = \frac{\partial \mathbf{B}}{\partial \mathbf{H}}(\mathbf{H}_0, \mathbf{T}_0), \quad \mathbf{d} = \frac{\partial \mathbf{B}}{\partial \mathbf{T}}(\mathbf{H}_0, \mathbf{T}_0),$$
$$\mathbf{s} = \frac{\partial \mathbf{S}}{\partial \mathbf{T}}(\mathbf{H}_0, \mathbf{T}_0), \quad \mathbf{d}^T = \frac{\partial \mathbf{S}}{\partial \mathbf{H}}(\mathbf{H}_0, \mathbf{T}_0). \tag{13}$$

The coefficients relating $\Delta\mathbf{B}, \Delta\mathbf{S}$ to $\Delta\mathbf{H}, \Delta\mathbf{T}$ can then be calculated

$$\begin{bmatrix} \boldsymbol{\mu}^{-1} & -\mathbf{a} \\ -\mathbf{a} & \mathbf{c} \end{bmatrix} = \begin{bmatrix} \boldsymbol{\mu} & \mathbf{d} \\ \mathbf{d} & \mathbf{s} \end{bmatrix}^{-1}. \tag{14}$$

A difficulty arising in this process is that the derivatives in (13) need to be calculated at $\mathbf{H}_0, \mathbf{T}_0$ (field and stress at the current time) which in the finite-element model are functions of $\mathbf{B}$ and $\mathbf{S}$, the unknowns. The process of calculating the coefficient matrices in (51) and (52) is iterative because available 3-D constitutive models [3]–[5] do not have an analytic inverse. It is therefore a vector process. All components of $\mathbf{H}_0$ and $\mathbf{T}_0$ must be calculated simultaneously with numerical inversion, using a technique such as the Newton-Raphson method. COMSOL Multiphysics does not have the capability of implementing vector functions so a single set of linear coefficients is used for the modeling in this section. To ensure that a linear material model is accurate, the actuator is operated about a bias field from a dc current; all reported values are referenced to this bias. The boundary conditions are $\mathbf{A} = 0$ on the air boundary and $\mathbf{u} = 0$ on the bottom face of the block used for mounting the beam.

D. Step Response Measurement and Dynamic Efficiency

First, a step response is measured by supplying a step input voltage source $V_s = 8.19$ volts to the coil. The finite-element model requires a source current density $\mathbf{J}_s$ as input. This density can be calculated in the circumferential direction from the dc resistance of the coil R and the cross sectional area of the coil wire A_w, $J_s = V_s/(RA_w)$. The coil is modeled as a solid cylinder with its center on the x_1-axis, so the 3-D supplied current density can be calculated from the circumferential component according to

$$\mathbf{J}_s = \begin{bmatrix} 0 \\ V_s/(RA_w) \times \left(-x_3/\sqrt{x_2^2 + x_3^2}\right) \\ V_s/(RA_w) \times \left(x_2/\sqrt{x_2^2 + x_3^2}\right) \end{bmatrix}. \tag{15}$$

Two quantities measured during the step response are compared with the model, the wire current in the coil and the vertical displacement of the beam tip (positive downward). The displacement is measured with a Keyence laser displacement sensor. The current is calculated as follows. The total current density is the sum of the source current density and the *back EMF*, or the opposing current/eddy current from the Lenz-Faraday law, $-\sigma\partial\mathbf{A}/\partial t$. The total circumferential current density then is

$$J(\mathbf{x}) = J_s - \sigma\frac{\partial A_2}{\partial t}\left(-\frac{x_3}{\sqrt{x_2^2 + x_3^2}}\right) - \sigma\frac{\partial A_3}{\partial t}\left(\frac{x_2}{\sqrt{x_2^2 + x_3^2}}\right) \tag{16}$$

and the wire current I in the coil is then calculated from the average circumferential current density $\bar{J}$ averaged over the coil, $I = \bar{J}A_w$. The vertical displacement is calculated from the model by averaging the vertical displacement of the top edge of the Galfenol layer on the free end.

The elastic modulus of the brass substrate is 120 GPa and its density is 8400 kg/m^3. The elastic modulus of the steel base is 200 GPa and its density is 7860 kg/m^3. The electrical conductivity of copper is $\sigma_C = 59.6 \times 10^6$ S/m. However, this is scaled by $\pi/4$ since there are voids within the coil winding with copper taking up $\pi/4$ of the cross section (the ratio of the area of a circle to the area of a square). The conductivity of the brass substrate is $0.28\sigma_C$ and both steel and Galfenol have conductivities of $0.1\sigma_C$. The permeability of the steel flux path is isotropic, $10 \times 10^3\ \mu_0$. The base for clamping the beam is made of nonmagnetic steel; a permeability of μ_0 is assumed. Brass is also nonmagnetic.

Model and experiment step responses are shown in Fig. 2. The voltage response is typical of a linear inductor-resistor electrical circuit and is described accurately by the model. The voltage step gives an impact-like input to the mechanical domain of the system through magnetomechanical coupling. As a result, the fundamental mode is excited and observed in both the measurement and the simulation. The fundamental frequency of the 3-D beam is the same as the measured frequency, 620 Hz, which also agrees with Euler beam theory.

A power efficiency study of the unimorph actuator shows that the two greatest sources of inefficiency are the power loss to the back EMF of the coil and the power loss due to flux leakage in the air. From (8), the input power to the system is

$$P_{\text{input}} = \int_{V_{\text{coil}}} \mathbf{J}_s \cdot \dot{\mathbf{A}}\, dV \tag{17}$$

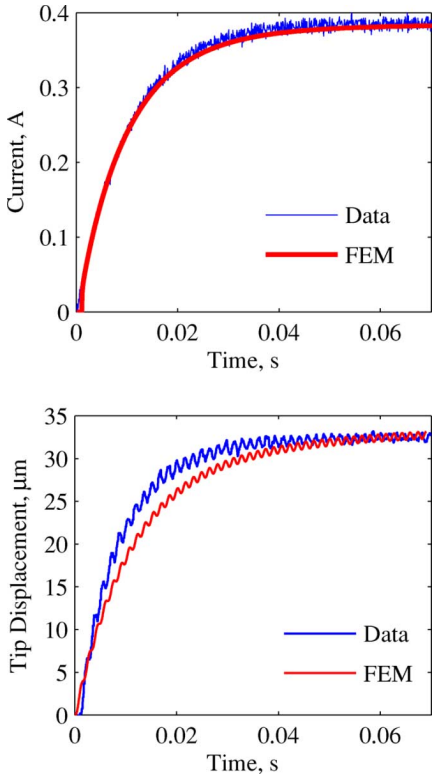

Fig. 2. Voltage step response of unimorph actuator with 8.22 volts input.

where the variation is replaced with a time derivative. The input power is expended in the magnetic power of each subdomain D

$$P^D_{\text{magnetic}} = \int_{V_D} \mathbf{H} \cdot \dot{\mathbf{B}}\, dV \tag{18}$$

and in the dynamic losses of each subdomain

$$P^D_{\text{loss}} = \int_{V_D} \sigma \dot{\mathbf{A}} \cdot \dot{\mathbf{A}}\, dV. \tag{19}$$

The most significant power sinks are plotted with the power source in Fig. 3(a). At the beginning of the step response, nearly all of the power is consumed in dynamic losses. Fig. 3(b) shows the total dynamic losses $\sum P^D_{\text{loss}}$ along with losses $P^{\text{coil}}_{\text{loss}}$, $P^{\text{Galfenol}}_{\text{loss}}$, and $P^{\text{steel}}_{\text{loss}}$. The most significant loss is in the coil which is the back EMF, followed by the steel and a negligible amount in the Galfenol driver. The most significant power sinks are shown as a fraction of input power in Fig. 4. This shows that initially, the back EMF accounts for nearly all of the power consumption. As the system approaches steady-state P^D_{magnetic} begins to dominate with $P^{\text{air}}_{\text{magnetic}}$, flux leakage to air, accounting for 65% of the power. The magnetic power supplied to the Galfenol driver, P^D_{magnetic} accounts for at most 5% of the power consumption.

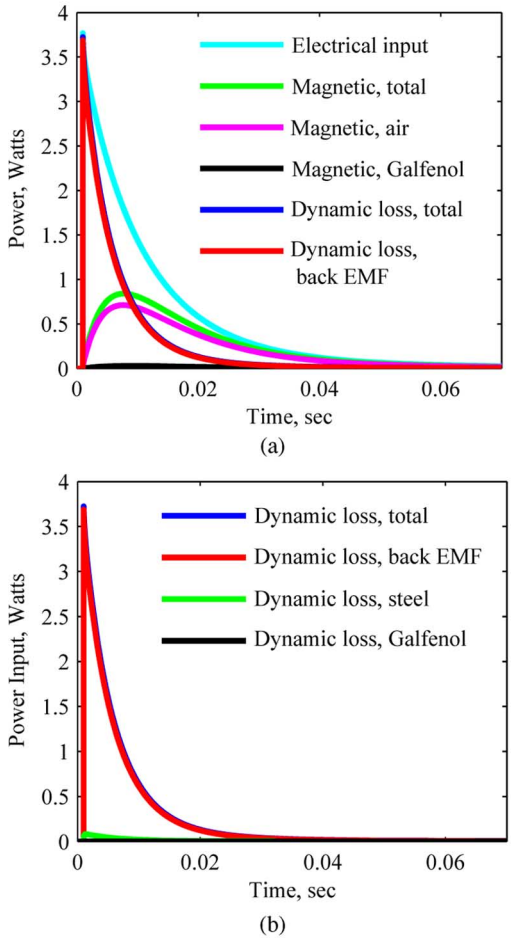

Fig. 3. Power consumption during voltage step input. (a) Power input and sinks; (b) dynamic losses due to coil back EMF and eddy currents in steel parts and Galfenol driver.

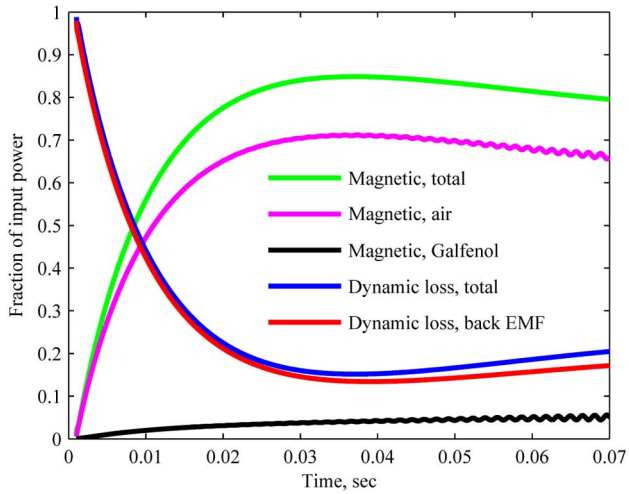

Fig. 4. Power consumption as a fraction of input power during voltage step input.

E. Quasi-Static Power Efficiency

A quasi-static simulation (0.1 Hz) provides more detail regarding the power loss to flux leakage in the air, $P^{\text{air}}_{\text{magnetic}}$. Additionally, it demonstrates the capability of the 3-D finite-element model to calculate the spatial dependence of the flux density (Fig. 8), magnetic field (Fig. 9), strain (Fig. 10), and stress (Fig. 11).

The power traces P_{input}, $\sum P^D_{\text{magnetic}}$, $P^{\text{air}}_{\text{magnetic}}$, $P^{\text{Galfenol}}_{\text{magnetic}}$, and $\sum P^D_{\text{loss}}$ are shown in Fig. 5 and the same power sinks are

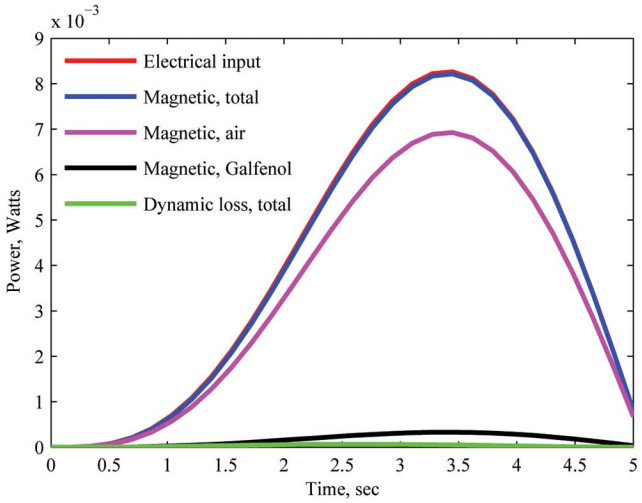

Fig. 5. Quasi-static (0.1 Hz) power consumption.

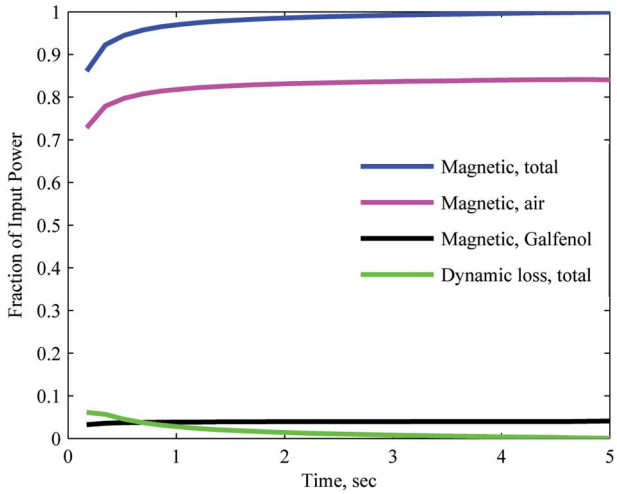

Fig. 6. Quasi-static (0.1 Hz) power consumption as a fraction of power input.

shown as a fraction of P_{input} in Fig. 6. Flux leakage to the air accounts for 82% of the input power while only 5% is supplied to the Galfenol driver. The conversion efficiency of magnetic energy into mechanical energy of the Galfenol driver is calculated from the magnetomechanical coupling

$$K = \frac{\int_{V_{\text{Galfenol}}} -\mathbf{a}\mathbf{S}\cdot\dot{\mathbf{B}}\,dV + \int_{V_{\text{Galfenol}}} -\mathbf{a}^T\mathbf{B}\cdot\dot{\mathbf{S}}\,dV}{\sqrt{\int_{V_{\text{Galfenol}}} \boldsymbol{\mu}^{-1}\mathbf{B}\cdot\dot{\mathbf{B}}\,dV \int_{V_{\text{Galfenol}}} \mathbf{c}\mathbf{S}\cdot\dot{\mathbf{S}}\,dV}}. \quad (20)$$

The conversion efficiency is a function of geometry, coupling matrix $\mathbf{a}$, permeability $\boldsymbol{\mu}$, and stiffness $\mathbf{c}$. This calculation is shown in Fig. 7. The conversion efficiency is close to 50%, however this analysis shows that the efficiency of the overall system is poor since only 5% of the input power is supplied to the Galfenol layer, which in turn has a near 50% conversion efficiency. The geometry of the actuator is therefore the chief reason for the poor efficiency. It can be improved by reducing the air gap thereby reducing flux leakage or improving the coil geometry to reduce the back EMF. Ideally, the flux path should

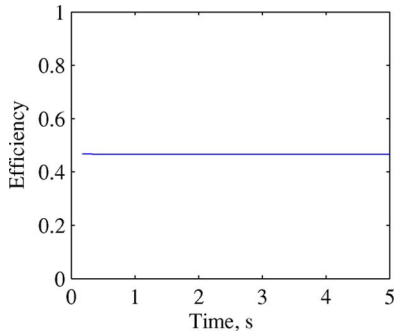

Fig. 7. Magnetomechanical coupling efficiency.

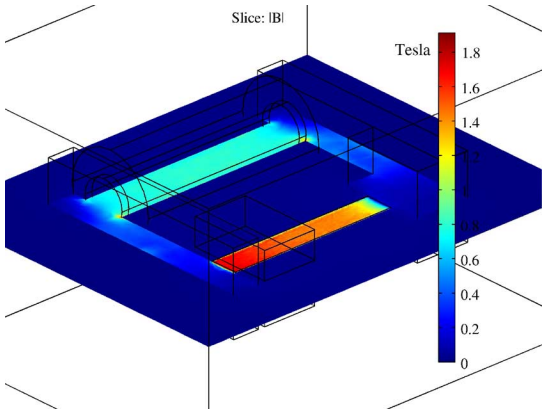

Fig. 8. FEM solution for flux density.

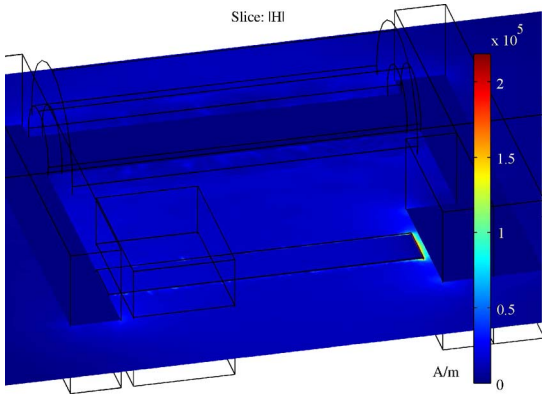

Fig. 9. FEM solution for magnetic field.

not include air since its permeability is much lower than the permeability of Galfenol. Additionally, a long narrow coil is generally more efficient than a short wide coil.

III. Concluding Remarks

The finite-element method was employed to describe the spatial and temporal dependence of the flux density, strain or displacement, magnetic field, and stress in 3-D magnetostrictive transducers. A general formulation was developed for magnetostrictive transducers which allows for subdomains to have different degrees of freedom. The virtual work was derived from the strong form or partial differential equation

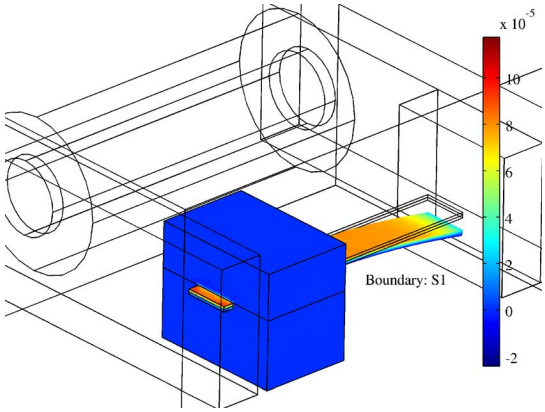

Fig. 10. FEM solution for strain.

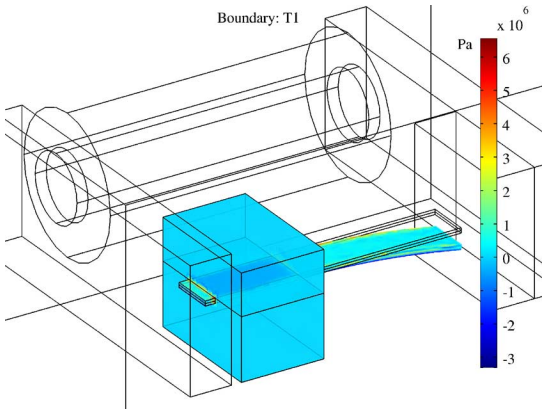

Fig. 11. FEM solution for stress.

description, without the use of assumptions such as linearity on the material constitutive behavior.

A fully 3-D and dynamic implementation was used to study the magnetoelastic response and efficiency of a unimorph actuator. From the virtual work, expressions were developed for the input power, magnetic field power, and power lost to eddy currents. Furthermore, a method for calculating the magnetomechanical energy conversion efficiency was developed which includes geometry dependence. For this particular design, it was shown that the geometry of the transducer is not optimal compared to the coupling efficiency of Galfenol, shown to be nearly 50%. The analysis permits to quantify the adverse effects of back EMF, eddy currents, and flux leakage in 3-D.

Appendix A
Derivation of Weak Form Equations of Multiple Subdomains

The weak form is derived in a straightforward manner utilizing indicial notation and defining the permutation tensor

$$\epsilon_{ijk} = \begin{cases} 1, \text{ clockwise sequence } (123, 231, 312) \\ -1, \text{ counter}-\text{clockwise sequence } (321, 213, 132) \\ 0, \text{ any two indices equal} \end{cases}. \tag{21}$$

Using the permutation tensor, the cross-product is $(\mathbf{a} \times \mathbf{b})_i = \epsilon_{ijk} a_j b_k$ and the curl is $(\nabla \times \mathbf{a})_i = \epsilon_{ijk} \partial a_k / \partial x_j$. Also, switching the order gives $\epsilon_{ijk} a_k b_j = -\epsilon_{ijk} a_j b_k$. In Einstein notation, the equations to be solved are

$$\epsilon_{ijk} \frac{\partial H_k}{\partial x_j} = (J_s)_i - \sigma \frac{\partial A_i}{\partial t} \tag{22}$$

$$\rho \frac{\partial^2 u_i}{\partial t^2} + c \frac{\partial u_i}{\partial t} = \frac{\partial T_{ij}}{\partial x_j} + (f_B)_i. \tag{23}$$

Flux density is kinematically related to vector magnetic potential and strain to displacement. The magnetic field in (22) is related, by a material constitutive law, to flux density and strain, if the material is magnetostrictive, or simply to the flux density for passive materials or free space. The stress in (23) is also related to flux density and strain for magnetostrictive materials. For passive materials the stress is only related to the strain. With the kinematic relationships and the material constitutive laws, the two initial boundary value problems (22) and (23) can be formulated with dependent variables vector magnetic potential and displacement and source terms current density and body force. Essential boundary conditions are specified vector potential and displacement. A typical system to be solved is surrounded by an air volume, chosen sufficiently large so that $A_i = 0$ on the boundary. In the weak form, the natural boundary conditions emerge as work terms applied to material boundaries, arising from the tangential component of magnetic fields applied at the boundary and the traction force $\mathbf{t}$ applied to the boundary.

The weak form is derived from the method of weighted residuals applied to (22) and (23)

$$\int_{V_B} \epsilon_{ijk} \frac{\partial H_k}{\partial x_j} \psi_i \, dV + \int_{V_B} \sigma \frac{\partial A_i}{\partial t} \psi_i \, dV = \int_{V_B} (J_s)_i \psi_i \, dV \tag{24}$$

$$- \int_{V_u} \frac{\partial T_{ij}}{\partial x_j} \varphi_i \, dV + \int_{V_u} \rho \frac{\partial^2 u_i}{\partial t^2} \varphi_i \, dV + \int_{V_u} c \frac{\partial u_i}{\partial t} \varphi_i \, dV = \int_{V_u} (f_B)_i \varphi_i \, dV \tag{25}$$

where ψ_i and φ_i are kinematically admissible test functions (zero where essential boundary conditions exist.) The volumes V_B and V_u are the subdomains for which flux density and mechanical displacement are defined, respectively. Consider for example the hypothetical system in Fig. 12. The displacement volume consists of the magnetostrictive material and the steel flux path, which is deformed by the magnetostrictive material and by externally applied traction forces. The flux density volume consists of the entire domain since the current-carrying coil results in flux density over the entire domain.

Integration by parts gives for the first terms in (24) and (25)

$$\int_{V_B} \epsilon_{ijk} \frac{\partial H_k}{\partial x_j} \psi_i \, dV = \int_{V_B} \epsilon_{ijk} \left[\frac{\partial (H_k \psi_i)}{\partial x_j} - H_k \frac{\partial \psi_i}{\partial x_j} \right] dV \tag{26}$$

$$- \int_{V_u} \frac{\partial T_{ij}}{\partial x_j} \varphi_i \, dV = - \int_{V_u} \left[\frac{\partial (T_{ij} \varphi_i)}{\partial x_j} - T_{ij} \frac{\partial \varphi_i}{\partial x_j} \right] dV. \tag{27}$$

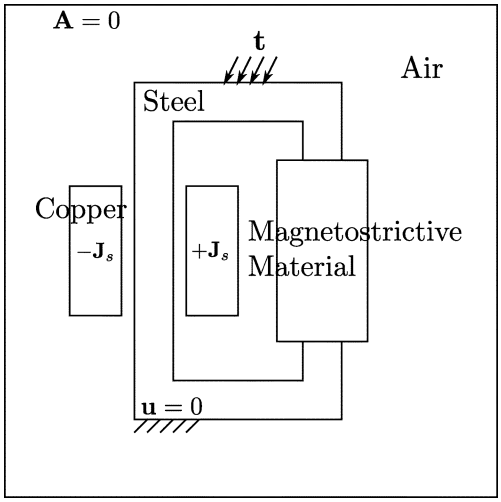

Fig. 12. Hypothetical system with a magnetostrictive material, flux return path, and drive coil in an air volume.

Applying the divergence theorem to the first term in each of the above gives

$$\int_{V_B} \epsilon_{ijk} \frac{\partial (H_k \psi_i)}{\partial x_j}\, dV = \int_{\partial V_B} \epsilon_{ijk} H_k \psi_i n_j d\partial V \quad (28)$$

$$\int_{V_u} \frac{\partial (T_{ij} \varphi_i)}{\partial x_j}\, dV = \int_{\partial V_u} T_{ij} \varphi_i n_j d\partial V. \quad (29)$$

Substitution of these relations into (24) and (25) along with $\epsilon_{ijk} H_k \partial \psi_i / \partial x_j = -\epsilon_{ijk} H_i \partial \psi_k / \partial x_j$ and $\epsilon_{ijk} H_k \psi_i n_j = -\epsilon_{ijk} H_j n_k \psi_i$, gives

$$\int_{V_B} H_i \epsilon_{ijk} \frac{\partial \psi_k}{\partial x_j}\, dV + \int_{V_B} \sigma \frac{\partial A_i}{\partial t} \psi_i\, dV = \int_{\partial V_B} \epsilon_{ijk} H_j n_k \psi_i d\partial V + \int_{V_B} (J_s)_i \psi_i\, dV \quad (30)$$

$$\int_{V_u} T_{ij} \frac{\partial \varphi_i}{\partial x_j}\, dV + \int_{V_u} \rho \frac{\partial^2 u_i}{\partial t^2} \varphi_i\, dV + \int_{V_u} c \frac{\partial u_i}{\partial t} \varphi_i\, dV = \int_{\partial V_u} T_{ij} \varphi_i n_j d\partial V + \int_{V_u} (f_B)_i \varphi_i\, dV. \quad (31)$$

In the Galerkin method, the weighting functions have the same basis as the dependent functions which in this case are A_i and u_i. The weighting functions can also be thought of as virtual generalized displacements, $\psi_i = \delta A_i$ and $\varphi_i = \delta u_i$. The weak form, in Einstein notation, is then

$$\int_{V_B} H_i \epsilon_{ijk} \frac{\partial \delta A_k}{\partial x_j}\, dV + \int_{V_B} \sigma \frac{\partial A_i}{\partial t} \delta A_i\, dV = \int_{\partial V_B} \epsilon_{ijk} H_j n_k \delta A_i d\partial V + \int_{V_B} (J_s)_i \delta A_i\, dV \quad (32)$$

$$\int_{V_u} T_{ij} \frac{\partial \delta u_i}{\partial x_j}\, dV + \int_{V_u} \rho \frac{\partial^2 u_i}{\partial t^2} \delta u_i dV + \int_{V_u} c \frac{\partial u_i}{\partial t} \delta u_i\, dV = \int_{\partial V_u} T_{ij} n_j \delta u_i d\partial V + \int_{V_u} (f_B)_i \delta u_i\, dV \quad (33)$$

or in matrix notation

$$\int_{V_B} \mathbf{H} \cdot (\nabla \times \delta \mathbf{A})\, dV + \int_{V_B} \sigma \frac{\partial \mathbf{A}}{\partial t} \cdot \delta \mathbf{A}\, dV = \int_{\partial V_B} (\mathbf{H} \times \mathbf{n}) \cdot \delta \mathbf{A}\, d\partial V + \int_{V_B} \mathbf{J}_s \cdot \delta \mathbf{A}\, dV \quad (34)$$

$$\int_{V_u} \mathbf{T} \cdot \nabla \delta \mathbf{u}\, dV + \int_{V_u} \rho \frac{\partial^2 \mathbf{u}}{\partial t^2} \cdot \delta \mathbf{u}\, dV + \int_{V_u} c \frac{\partial \mathbf{u}}{\partial t} \cdot \delta \mathbf{u}\, dV = \int_{\partial V_u} \mathbf{T}\mathbf{n} \cdot \delta \mathbf{u}\, d\partial V + \int_{V_u} \mathbf{f}_B \cdot \delta \mathbf{u}\, dV. \quad (35)$$

APPENDIX B
FINITE-ELEMENT ASSEMBLY FOR COUPLED SYSTEMS

The interpolations and integrations, performed over element number e, are done in local or natural coordinates $\boldsymbol{\xi}$ with Jacobian $\boldsymbol{\mathcal{J}}_e$ relating the differential $d\mathbf{x}$ to $d\boldsymbol{\xi}$ so that $d\mathbf{x} = \boldsymbol{\mathcal{J}}_e d\boldsymbol{\xi}$ and $dV = \det(\boldsymbol{\mathcal{J}}_e) d\xi_1 d\xi_2 d\xi_3 = J_e d\xi_1 d\xi_2 d\xi_3$. For a linearly interpolated geometry, the spatially dependent $\mathbf{A}_e$ and $\mathbf{u}_e$ in an element are interpolated from the nodal values $\mathbf{q}_e^A$ and $\mathbf{q}_e^u$ according to

$$\mathbf{A}_e = \mathbf{N}_A(\boldsymbol{\xi}) \mathbf{q}_e^A,\ \mathbf{u}_e = \mathbf{N}_u(\boldsymbol{\xi}) \mathbf{q}_e^u. \quad (36)$$

Since the virtual quantities have the same basis in the Galerkin method, the same shape functions are used for the virtual quantities

$$\delta \mathbf{A}_e = \mathbf{N}^A(\boldsymbol{\xi}) \delta \mathbf{q}_e^A,\ \delta \mathbf{u}_e = \mathbf{N}^u(\boldsymbol{\xi}) \delta \mathbf{q}_e^u. \quad (37)$$

As shown above, $\mathbf{A}_e$ and $\mathbf{u}_e$ need not have the same element type or interpolation matrix. The interpolation matrix $\mathbf{N}^A$ has three rows, since $\mathbf{A}$ is a 3-D vector, and for an element having N_n^A nodes (N_n^A depends on the element order) it has N_q^A columns where $N_q^A = 3N_n^A$, since each node has an associated 3-D vector containing the nodal value of $\mathbf{A}_e$. The vector $\mathbf{q}_e^A$ has N_q^A entries which correspond to the three components of $\mathbf{A}_e$ at each node. Since the displacements need not have the same shape functions, $\mathbf{N}^u$ has N_q^u columns which depends on the number of nodes N_n^u. The total degrees of freedom for an element is therefore $N_q = N_q^u + N_q^A$.

Typical choices for the shape functions are linear or quadratic Lagrange shape functions employed over tetrahedral elements. Eight-node brick elements may also be used but are more challenging to implement because of a lack of robust meshing algorithms. If 4-node tetrahedral elements are used for both vector potential and displacement, then $\mathbf{N}^A = \mathbf{N}^q = \mathbf{N}$. A tetrahedral element using linear shape functions has four nodes (see Fig. 13). The matrix shape function $\mathbf{N}$ is comprised of the Lagrange shape functions

$$N_1 = \xi_1, \quad (38)$$

$$N_2 = \xi_2, \quad (39)$$

$$N_3 = \xi_3, \quad (40)$$

$$N_4 = 1 - \xi_1 - \xi_2 - \xi_3. \quad (41)$$

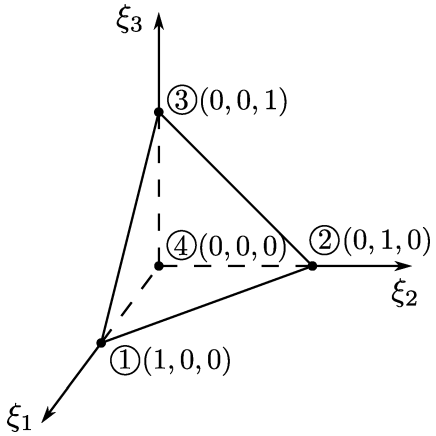

Fig. 13. 4-node tetrahedral element.

Shape functions have the property that at node i, $N_j = 1$ for $j = i$ and $N_j = 0$ for $j \neq i$ and are thus used to interpolate both the geometry and the solution variables. For example, the spatial coordinate x_1 is interpolated from the nodal values $x_{1,n}$ in the following manner:

$$x_1 = N_1 x_{1,1} + N_2 x_{1,2} + N_3 x_{1,3} + N_4 x_{1,4}. \tag{42}$$

The vector $\mathbf{q}_e^A$ has twelve entries, the first three are the three components of $\mathbf{A}_e$ at node 1, the second three are the components at node 2 and likewise for the remaining two nodes. It follows that the shape function matrix is

$$\mathbf{N}(\boldsymbol{\xi}) = \begin{bmatrix} N_1 & 0 & 0 & N_2 & 0 & 0 \\ 0 & N_1 & 0 & 0 & N_2 & 0 \\ 0 & 0 & N_1 & 0 & 0 & N_2 \\ N_3 & 0 & 0 & N_4 & 0 & 0 \\ 0 & N_3 & 0 & 0 & N_4 & 0 \\ 0 & 0 & N_3 & 0 & 0 & N_4 \end{bmatrix} \tag{43}$$

so that when $\boldsymbol{\xi} = (1, 0, 0)$ or at node 1, $\mathbf{A}_e = \mathbf{A}_{e,1}$; the vector potential is simply the value at node 1. Likewise when $\boldsymbol{\xi} = (0, 1, 0)$ or at node 2, $\mathbf{A}_e = \mathbf{A}_{e,2}$; the vector potential is simply the value at node 2 and similarly for the other nodes. Elsewhere in the tetrahedron, the shape functions simply result in a linear interpolation of the nodal values. For example, if $\boldsymbol{\xi} = (1/2, 1/2, 0)$ which lies midway along the edge connecting nodes 1 and 2, $\mathbf{A}_e = (1/2)(\mathbf{A}_{e,1} + \mathbf{A}_{e,2})$.

In the finite-element model, the nodal values of the vector potential and displacement are the unknowns and the nodal values of the virtual vector potential and displacement are arbitrary. To include the finite-element discretization in the virtual work (8) and (9), the flux density, magnetic field, strain, and stress need to be calculated from the vector potential and displacement

$$\mathbf{B}_e = \nabla \times \mathbf{A}_e = \nabla \times \left(\mathbf{N}^A \mathbf{q}_e^A\right) := \mathbf{C}_e \mathbf{q}_e^A \tag{44}$$

$$\mathbf{S}_e = \nabla \mathbf{u}_e = \nabla \left(\mathbf{N}^u \mathbf{q}_e^u\right) := \mathbf{G}_e \mathbf{q}_e^u. \tag{45}$$

The entries in the matrices $\mathbf{C}_e$ and $\mathbf{G}_e$ contain the derivatives of the local coordinate system $\boldsymbol{\xi}$ with respect to the global coordinate system $\mathbf{x}$ and can be thought of as the discrete form of the curl and gradient operators. For linear elements they do not depend on $\boldsymbol{\xi}$ since the Jacobian $\boldsymbol{\mathcal{J}}$ is a constant matrix containing the side lengths of the tetrahedral element, however for higher order elements including the quadratic element they depend on $\boldsymbol{\xi}$. Making the substitutions and performing the integrals over N^A elements for the magnetic domain and N^u elements for the mechanical domain results in the following summations for the virtual work balance

$$\sum_{e=1}^{N^A} \left(\int_\Delta \mathbf{H}_e \cdot \delta \mathbf{B}_e \, J_e d\Delta + \int_\Delta \sigma_e \frac{\partial \mathbf{A}_e}{\partial t} \cdot \delta \mathbf{A}_e \, J_e d\Delta \right) = \sum_{b=1}^{N_S^A} \int_\Delta \mathbf{H}_{T,b} \cdot \delta \mathbf{A}_b \, J_{b,S} d\Delta_S + \sum_{e=1}^{N^A} \int_\Delta \mathbf{J}_{s,e} \cdot \delta \mathbf{A}_e \, J_e d\Delta, \tag{46}$$

$$\sum_{e=1}^{N^u} \left(\int_\Delta \mathbf{T}_e \cdot \delta \mathbf{S}_e \, J_e d\Delta + \int_\Delta \rho_e \frac{\partial^2 \mathbf{u}_e}{\partial t^2} \cdot \delta \mathbf{u}_e \, J_e d\Delta + \int_\Delta c_e \frac{\partial \mathbf{u}_e}{\partial t} \cdot \delta \mathbf{u}_e \, J_e d\Delta \right) = \sum_{b=1}^{N_S^u} \int_{\Delta_S} \mathbf{t}_b \cdot \delta \mathbf{u}_b \, J_{b,S} d\Delta_S. \tag{47}$$

The body force term has been dropped since the effects of gravity and the electromagnetic Lorentz forces are usually negligible in magnetostrictive devices [18]. The subscript b refers to the element number on the boundary; there are N_S^A for the magnetic domain and N_S^u for the mechanical domain which have an applied magnetic field and an applied traction, respectively. The integral $\int_\Delta J_e \, d\Delta$ refers to the integral over the element in natural coordinates and is the volume of the element

$$\int_\Delta J_e d\Delta := \int_{-1}^{1} \int_{-1}^{1} \int_{-1}^{1} \det\left(\frac{\partial \mathbf{x}}{\partial \boldsymbol{\xi}}\right) d\xi_1 d\xi_2 d\xi_3 = V_e \tag{48}$$

and the integral $\int_{\Delta_S} J_{b,S} \, d\Delta_S$ gives the surface area of the element face on the boundary

$$\int_{\Delta_S} J_{b,S} \, d\Delta_S := \int_{-1}^{1} \int_{-1}^{1} \det \begin{bmatrix} \frac{\partial x_i}{\partial \xi_i} & \frac{\partial x_i}{\partial \xi_j} \\ \frac{\partial x_j}{\partial \xi_i} & \frac{\partial x_j}{\partial \xi_j} \end{bmatrix} d\xi_i d\xi_j = A_b. \tag{49}$$

Point loads can be included in a very straightforward manner if they are applied at element nodes. For point force $\mathbf{P}_p$ applied at node p, the virtual work is $\mathbf{P}_p \cdot \delta \mathbf{q}_p^u$, so for N_p^u point loads, the following should be added to the right-hand side of the mechanical virtual work balance

$$\sum_{p=1}^{N_p^u} \mathbf{P}_p \cdot \delta \mathbf{q}_p^u. \tag{50}$$

Incorporation of Constitutive Laws: Galfenol constitutive behavior of magnetic field and stress versus flux density and strain is nonlinear. This nonlinearity is the only such in the finite-element model developed in this work. All other materials considered have linear constitutive behavior, governed mechanically by Hooke's law and magnetically by a constant, isotropic permeability. Geometric nonlinearities are not considered here. It may be necessary to include geometric nonlinearities in order

to model manufacturing processes involving plastic strains. In this case, a plastic, nonlinear stress versus strain relationship would be needed as well as the use of finite strains which are nonlinearly related to displacement. The finite-element model developed here is applicable to transducers which are operated in the elastic region where the only source of nonlinearity in the stress versus strain relationship is the magnetostriction. In the Newton-Raphson method for solving nonlinear problems, the problem is linearized and solved iteratively for the increments from the initial condition. For small enough increments, the constitutive law for Galfenol and magnetostrictive materials in general is

$$\Delta\mathbf{H} = \boldsymbol{\mu}^{-1}\Delta\mathbf{B} - \mathbf{a}\Delta\mathbf{S} \tag{51}$$

$$\Delta\mathbf{T} = -\mathbf{a}^T\Delta\mathbf{B} + \mathbf{c}\Delta\mathbf{S}. \tag{52}$$

The permeability matrix $\boldsymbol{\mu}$ is the permeability at constant $\mathbf{S}$ and the stiffness matrix $\mathbf{c}$ is the stiffness at constant $\mathbf{B}$. Magnetically-induced stress and mechanically-induced magnetic field arise from the magnetomechanical coupling matrix $\mathbf{a}$. For passive materials in the magnetic domain, (51) is used with $\mathbf{a} = \mathbf{0}$. For passive materials in the mechanical domain, (52) is used with $\mathbf{a} = \mathbf{0}$. The importance of partitioning the total domain to be analyzed into magnetic and mechanical subdomains can be understood from the constitutive law. Consider for example the air volume which does not have an enclosure and is hence free to move. The permeability is simply μ_0 and the stiffness is essentially zero compared to other media in the domain such as copper, steel, and Galfenol. To illustrate, the Galfenol driver does no work if it deflects while pushing against air. The situation would be different if the air were enclosed in an acoustic chamber. In that case, air pressure would need to be considered and the air would be characterized by its bulk modulus. Acoustic-structural interactions are not addressed in this work. Integrating the virtual work for both magnetic and mechanical quantities over the entire domain would give the same amount of work as first partitioning and then integrating only over media which have non-zero stiffness for the mechanical virtual work. This is because media with zero stiffness introduce no mechanical virtual work. While both approaches lead to the same virtual work, performing the integration and element summation over the entire domain will lead to a singular stiffness matrix in practice, resulting in a non-unique solution.

In the incremental solution, solution starts from an initial state which is known and $\mathbf{q}_e^A$ and $\mathbf{q}_e^u$ are the vector potential and displacement increments. Additionally, the input quantities traction $\mathbf{t}$, surface field $\mathbf{H}_T$ and source current density $\mathbf{J}_s$ are increments. In incremental form, the linear constitutive laws can be used to relate increments of magnetic field and stress to the finite-element solution

$$\mathbf{H}_e = \boldsymbol{\mu}_e^{-1}\mathbf{C}_e\mathbf{q}_e^A - \mathbf{a}_e\mathbf{G}_e\mathbf{q}_e^u \tag{53}$$

$$\mathbf{T}_e = -\mathbf{a}_e^T\mathbf{C}_e\mathbf{q}_e^A + \mathbf{c}_e\mathbf{G}_e\mathbf{q}_e^u. \tag{54}$$

These relations can now be substituted into the finite-element approximation for the virtual work given by (46) and (47). This yields matrix equations for increments of the vector potential and displacement nodal values, since they can be pulled from the integral. To illustrate, the following matrices are defined:

$$\mathbf{k}_e^u = \int_\Delta \mathbf{G}_e^T\mathbf{c}_e\mathbf{G}_e J_e d\Delta \tag{55}$$

$$\mathbf{k}_e^A = \int_\Delta \mathbf{C}_e^T\boldsymbol{\mu}_e^{-1}\mathbf{C}_e J_e d\Delta \tag{56}$$

$$\mathbf{k}_e^{uA} = \int_\Delta \mathbf{C}_e^T\mathbf{a}_e\mathbf{G}_e J_e d\Delta \tag{57}$$

$$\mathbf{d}_e^A = \int_\Delta (\mathbf{N}^A)^T\sigma_e\mathbf{N}^A J_e d\Delta \tag{58}$$

$$\mathbf{d}_e^u = \int_\Delta (\mathbf{N}^u)^T c_e\mathbf{N}^u J_e d\Delta \tag{59}$$

$$\mathbf{m}_e = \int_\Delta (\mathbf{N}^u)^T\rho_e\mathbf{N}^u J_e d\Delta \tag{60}$$

and the following vectors are defined:

$$\mathbf{f}_b^u = \int_{\Delta_S} (\mathbf{N}^u)^T\mathbf{t}_\mathbf{b} J_{b,S} d\Delta_S \tag{61}$$

$$\mathbf{f}_b^A = \int_{\Delta_S} \left(\mathbf{N}^A\right)^T \mathbf{H}_T J_{b,S} d\Delta_S \tag{62}$$

$$\mathbf{f}_e^J = -\int_\Delta \left(\mathbf{N}^A\right)^T \mathbf{J}_{s,e} J_e d\Delta. \tag{63}$$

Substitution of (53)–(54) and (44)–(45) into (46)–(47) and applying these definitions, the finite-element approximations for the magnetic and mechanical virtual work balance are

$$\sum_{e=1}^{N^A}\left(\mathbf{d}_e^A\dot{\mathbf{q}}_e^A + \mathbf{k}_e^A\mathbf{q}_e^A - \mathbf{k}_e^{uA}\mathbf{q}_e^u\right)\cdot\delta\mathbf{q}_e^A = \sum_{e=1}^{N_A}\mathbf{f}_e^J\cdot\delta\mathbf{q}_e^A + \sum_{b=1}^{N_S^A}\mathbf{f}_b^A\cdot\delta\mathbf{q}_b^A \tag{64}$$

$$\sum_{e=1}^{N^u}\left(\mathbf{m}_e\ddot{\mathbf{q}}_e^u + \mathbf{d}_e^u\dot{\mathbf{q}}_e^u + \mathbf{k}_e^u\mathbf{q}_e^u - \left(\mathbf{k}_e^{uA}\right)^T\mathbf{q}_e^A\right)\cdot\delta\mathbf{q}_e^u = \sum_{b=1}^{N_S^u}\mathbf{f}_b^u\cdot\delta\mathbf{q}_b^u + \sum_{p=1}^{N_p^u}\mathbf{P}_p\cdot\delta\mathbf{q}_p^u. \tag{65}$$

The global assembly process takes into account element connectivity and replaces the summations with matrix operations (see [22, Ch. 3] or [23, Ch. 12] for details). After global assembly, the finite-element model is

$$\left(\mathbf{D}^A\dot{\mathbf{Q}}^A + \mathbf{K}^A\mathbf{Q}^A - \mathbf{K}^{uA}\mathbf{Q}^u\right)\cdot\delta\mathbf{Q}^A = \mathbf{F}^A\cdot\delta\mathbf{Q}^A \tag{66}$$

$$\left(\mathbf{M}^u\ddot{\mathbf{Q}}^A + \mathbf{D}^u\dot{\mathbf{Q}}^u + \mathbf{K}^u\mathbf{Q}^u - \mathbf{K}^{uA}\mathbf{Q}^u\right)\cdot\delta\mathbf{Q}^u = \mathbf{F}^u\cdot\delta\mathbf{Q}^u. \tag{67}$$

The vector $\mathbf{Q}^A$ contains the nodal values of the vector potential increments. In the meshing scheme and global assembly process, a mapping is created from the nodal values of an element $\mathbf{q}_e^A$ to an entry in $\mathbf{Q}^A$. Most nodes are shared between elements and therefore the total degrees of freedom due to vector potential, or the length of the vector $\mathbf{Q}^A$ is less than the product of the number of elements and the degrees of freedom of an element, $N_Q^A < N_e^A N_q^A$. Likewise, the length of the vector of nodal displacement increments is $N_Q^u < N_e^u N_q^u$. A typical

model uses thousands of elements to represent the magnetostrictive element which has twelve degrees of freedom for linear, tetrahedral elements. This illustrates the importance of using an efficient constitutive model since it must be separately evaluated for each degree of freedom of which there are tens of thousands.

The final incremental form of the finite-element model for the vector potential and displacement increments results from equating the coefficients of the virtual generalized displacement in (66) and (67), which can be done because these are arbitrary

$$\begin{bmatrix} \mathbf{0} & \mathbf{0} \\ \mathbf{0} & \mathbf{M}^u \end{bmatrix} \begin{pmatrix} \ddot{\mathbf{Q}}^A \\ \ddot{\mathbf{Q}}^u \end{pmatrix} + \begin{bmatrix} \mathbf{D}^A & \mathbf{0} \\ \mathbf{0} & \mathbf{D}^u \end{bmatrix} \begin{pmatrix} \dot{\mathbf{Q}}^A \\ \dot{\mathbf{Q}}^u \end{pmatrix} + \begin{bmatrix} \mathbf{K}^A & -\mathbf{K}^{uA} \\ -(\mathbf{K}^{uA})^T & \mathbf{K}^u \end{bmatrix} \begin{pmatrix} \mathbf{Q}^A \\ \mathbf{Q}^u \end{pmatrix} = \begin{pmatrix} \mathbf{F}^A \\ \mathbf{F}^u \end{pmatrix}. \quad (68)$$

The essential or Dirichlet boundary conditions must be incorporated in order to obtain a unique solution to the finite-element model (10). The essential boundary conditions are specified displacement and vector potential.

ACKNOWLEDGMENT

This work was supported by the Office of Naval Research under Grant N000140610530. The unimorph actuator was supplied by Etrema Products, Inc.

REFERENCES

[1] T. Ueno and H. Toshiro, "Two-DOF micro magnetostrictive bending actuator for wobbling motion," *IEEE Trans. Magn.*, vol. 44, no. 11, pp. 4078–4083, Nov. 2008.

[2] Z. Zhang, T. Ueno, and T. Higuchi, "Development of a magnetostrictive linear motor for microrobots using Fe-Ga (Galfenol) alloys," *IEEE Trans. Magn.*, vol. 45, no. 10, pp. 4598–4600, Oct. 2009.

[3] P. Evans and M. Dapino, "State-space constitutive model for magnetization and magnetostriction of Galfenol alloys," *IEEE Trans. Magn.*, vol. 44, no. 7, pp. 1711–1720, Jul. 2008.

[4] P. Evans and M. Dapino, "Efficient model for field-induced magnetization and magnetostriction of Galfenol," *J. Appl. Phys.*, vol. 105, no. 11, p. 113901, 2009.

[5] P. Evans and M. Dapino, "Efficient magnetic hysteresis model for field and stress application in magnetostrictive Galfenol," *J. Appl. Phys.*, vol. 107, no. 6, pp. 063906–063906-11, 2010.

[6] W. Panusittikorn and P. Ro, "Modeling and control of a magnetostrictive tool servo system," *J. Dyn. Syst., Meas. Control*, vol. 130, pp. 031 003–1, May 2008.

[7] J. Nealis and R. Smith, "Model-based robust control design for magnetostrictive transducers operating in hysteretic and nonlinear regimes," *IEEE Trans. Control Syst. Technol.*, vol. 15, no. 1, pp. 22–39, Jan. 2007.

[8] W. Oates and R. Smith, "Nonlinear optimal control techniques for vibration attenuation using magnetostrictive actuators," *J. Intell. Mater. Syst. Struct.*, vol. 19, no. 2, pp. 193–209, 2007.

[9] X. Tan and J. Baras, "Modeling and control of hysteresis in magnetostrictive actuators," *Automatica*, vol. 40, pp. 1469–1480, 2004.

[10] M. Dapino, R. Smith, and A. Flatau, "Structural magnetic strain model for magnetostrictive transducers," *IEEE Trans. Magn.*, vol. 36, no. 3, pp. 545–556, May 2000.

[11] W. Huang, B. Wang, S. Cao, Y. Sun, L. Weng, and H. Chen, "Dynamic strain model with eddy current effects for giant magnetostrictive transducer," *IEEE Trans. Magn.*, vol. 43, no. 4, pp. 1381–1384, Apr. 2007.

[12] N. Sarawate and M. Dapino, "A dynamic actuation model for magnetostrictive materials," *Smart Mater. Struct.*, vol. 17, p. 065013, 2008.

[13] G. Engdahl and A. Bergqvist, "Loss simulations in magnetostrictive actuators," *J. Appl. Phys.*, vol. 79, no. 8, pp. 4689–4691, 1996.

[14] O. Bottauscio, M. Chiampi, A. Lovisolo, P. Roccato, and M. Zucca, "Dynamic modeling and experimental analysis of Terfenol-D rods for magnetostrictive actuators," *J. Appl. Phys.*, vol. 103, p. 07F121, 2009.

[15] S. Datta, J. Atulasimha, C. Mudivarthi, and A. Flatau, "The modeling of magnetomechanical sensors in laminated structures," *Smart Mater. Struct.*, vol. 17, p. 025010, 2008.

[16] S. Datta, J. Atulasimha, C. Mudivarthi, and A. Flatau, "Modeling of magnetomechanical actuators in laminated structures," *J. Intell. Mater. Syst. Struct.*, vol. 20, no. 9, pp. 1121–1135, 2009.

[17] H. Zhou and Y. Zhou, "Vibration suppression of laminated composite beams using actuators of giant magnetostrictive materials," *Smart Mater. Struct.*, vol. 16, pp. 198–206, 2007.

[18] K. Kannan and A. Dasgupta, "A nonlinear Galerkin finite-element theory for modeling magnetostrictive smart structures," *Smart Mater. Struct.*, vol. 6, pp. 341–350, 1997.

[19] C. Mudivarthi, S. Datta, J. Atulasimha, and A. Flatau, "A bidirectionally coupled magnetoelastic model and its validation using a Galfenol unimorph sensor," *Smart Mater. Struct.*, vol. 17, 2008.

[20] J. Kim and E. Jung, "Finite element analysis for acoustic characteristics of a magnetostrictive transducer," *Smart Mater. Struct.*, vol. 14, pp. 1273–1280, 2005.

[21] J. Pérez-Aparicio and H. Sosa, "A continuum three-dimensional, fully coupled, dynamic, non-linear finite element formulation for magnetostrictive materials," *Smart Mater. Struct.*, vol. 13, pp. 493–502, 2004.

[22] T. Chandrupatla and A. Belegundu, *Introduction to Finite Elements in Engineering*, 3rd ed. Upper Saddle River, New Jersey: Prentice-Hall, 2002, 07458.

[23] K. Bathe, *Finite Element Procedures*. Upper Saddle River, New Jersey: Prentice Hall, 1996, 07458.